## Stability of Cubic Single Network Phases in Diblock Copolymer Melts

PENGYU CHEN, MAHESH K. MAHANTHAPPA, KEVIN D. DORFMAN\*

Department of Chemical Engineering and Materials Science, University of Minnesota – Twin Cities, 421 Washington Ave. SE, Minneapolis, MN 55455, USA.

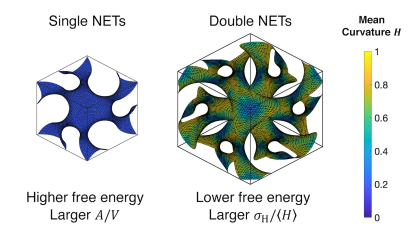
\*Corresponding Author: Kevin D. Dorfman. Email: dorfman@umn.edu. Phone: +1-612-624-5560. Fax: +1-612-626-7246.

Dated: June 27, 2022

**ABSTRACT:** We used self-consistent field theory (SCFT) to examine the stability of three cubic single network structures, single gyroid, single diamond, and single primitive, in neat diblock copolymer melts. Arguments related to packing frustration, as measured by the standard deviation in the mean curvature of the interface relative to its mean, that explain the relative stability of double gyroid, double diamond and double primitive also extend to the relative stability of their single networks. However, this packing frustration measure fails to account for the relative stabilities of single and double networks, e.g. single gyroid versus double gyroid, and arguments for a preferred curvature fail to explain the selection of double gyroid as the segregation strength increases. Rather, the larger interfacial areas per unit volume of single networks, arising from decreased domain sizes, are found to be a generic factor that leads to metastability of the cubic single networks relative to double gyroid in the network-forming region of the morphology diagram. These results clarify the origins of the metastability of single cubic network phases in neat diblock copolymer melts.

**Keywords:** SCFT, block copolymers, network phases, packing frustration, gyroid

#### TABLE OF CONTENTS



#### INTRODUCTION

The percolating 3D structures of polycontinuous mesoscale network phases (NETs) find wide-ranging applications as drug delivery vehicles, 1 structured electron and ion transporting media for energy conversion devices, <sup>2-4</sup> and size-selective separation membranes. <sup>5,6</sup> The most commonly observed NETs are the double gyroid (DG,  $Ia\bar{3}d$  symmetry), double diamond (DD,  $Pn\bar{3}m$  symmetry), and double primitive or "Plumber's Nightmare" (DP,  $Im\bar{3}m$ symmetry) phases.<sup>7,8</sup> These double NETs, which exhibit cubic symmetries, are tricontinuous phases comprising two interpenetrating and symmetry-equivalent networks of the same chemistry embedded within a matrix of a distinct chemical constitution. In AB diblock copolymers, these phases may be respectively conceptualized as arising from situating the B block termini (colored red in Figure 1) along either Schoen gyroid (G), Schwarz diamond (D), or Schwarz primitive (P) triply periodic minimal surfaces. 9 Some of these cubic double NETs are experimentally known to form in self-assembled block copolymers, <sup>8</sup> but single cubic networks such as the single gyroid (SG,  $I4_132$ ), single diamond (SD,  $Fd\bar{3}m$ ), and single primitive (SP,  $Pm\bar{3}m$ ) are yet to be observed, although self-consistent field theory (SCFT) has predicted SG could be self-assembled in linear pentablock copolymer melts. 10 As opposed to the double NETs, single NETs instead arise from situating the junctions of AB diblocks along the G, D, or P surfaces, thereby partitioning space into two discrete and interpenetrating volumes.

Cubic single NETs are of special interest due to their potentially unusual optical properties. The structural colors of butterfly wings<sup>11–13</sup> and beetle exoskeletons<sup>14</sup> arise from SG and SD structures, respectively, with cubic lattice parameters  $\geq$  100 nm. These structures have also captivated substantial interest as photonic materials with complete band gaps,

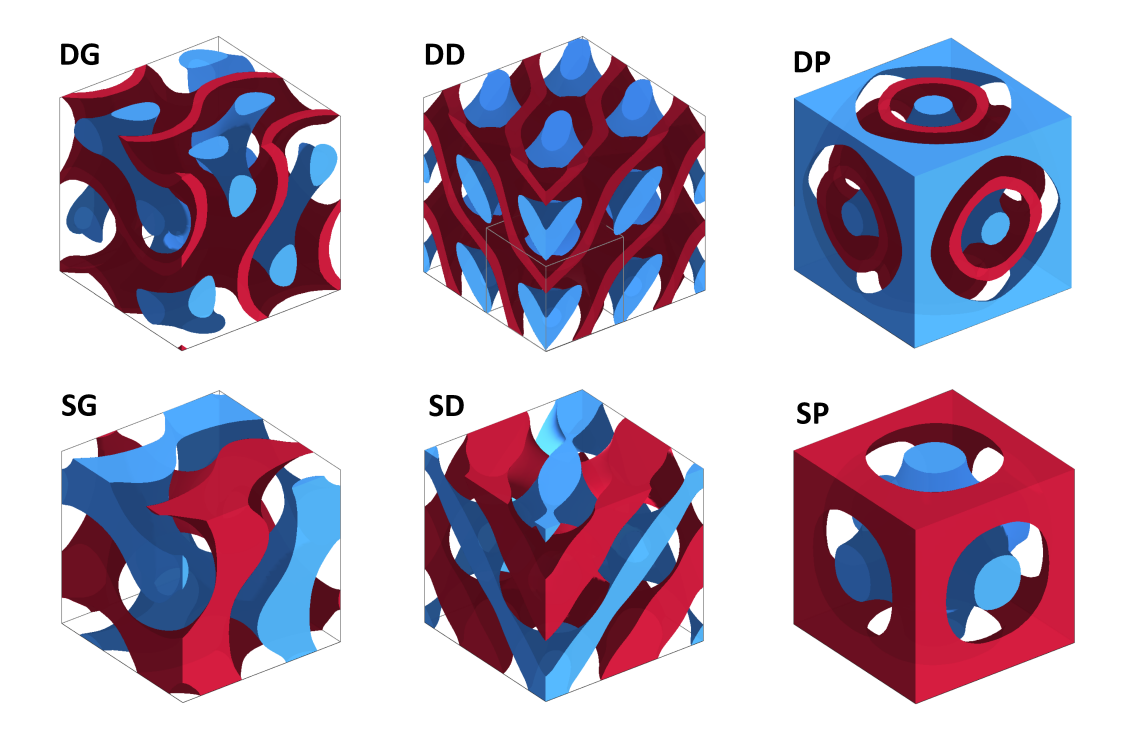


Figure 1: Composition profiles of cubic double and single NETs from converged self-consistent field theory (SCFT) solutions. Domains with different colors indicate differences in chemistry. The unit cell of DD is duplicated for easier visualization; the unit cell is indicated by the light gray boundaries. For the double networks, the two networks (in blue) and the dividing surface (in red) were created by plotting the network using a cutoff value of  $\phi_A > 0.9$  and the interface using a cutoff value of  $\phi_B > 0.95$ , with one exception for DP where the networks are displayed by using  $\phi_A > 0.5$ . For the single networks, each network is displayed by using  $\phi_A > 0.9$  (for the blue network) and  $\phi_B > 0.9$  (for the red network).

as predicted by calculations.<sup>15</sup> Additionally, SG nanostructures offer exciting opportunities to produce optical metamaterials<sup>16</sup> and chiroptical materials with demonstrably strong circular dichroism responses.<sup>17</sup> Advancing fundamental studies and future applications of light-matter interactions of these single NETs motivates investigations of methods for their fabrication with cubic lattice parameters ranging from 20-500 nm from a palette of materials with varied dielectric properties.

None of the cubic single NETs has been observed as an equilibrium phase in linear AB diblock copolymer melts, the simplest such system, and our goal here is to provide a basis

for this metastability via SCFT. Microstructure formation in block copolymers is governed by the competition between the enthalpic penalty for dissimilar polymer contacts and the entropy loss from chain stretching to minimize interfacial contacts. Based on the pioneering theoretical study by Matsen and Bates, packing frustration has been recognized as a major factor that hinders the formation of NETs in block copolymers. 18,19 Interfacial tension drives the block copolymer melt towards an ordered morphology with a smaller interfacial surface area between domains, whereas space filling at constant density with minimal variations in chain stretching prefers uniform domain thicknesses. Unlike the classical lamellar (L), cylinder (C), and spherical (S) phases, the cubic double NETs suffer from significant chain-stretching penalities inside the network nodes by virtue of deviations from a constant mean curvature. 20 The degree of packing frustration has thus been assessed by the deviation from the constant mean-curvature (CMC) geometry, as quantified by the relative variation in mean curvature  $\sigma_{\rm H}/\langle H \rangle$  of the domain interface, where  $\sigma_{\rm H}$  is the standard deviation and  $\langle H \rangle$  is the area-averaged Helfrich mean curvature. <sup>19</sup> By applying this calculation, it has been shown that the degree of packing frustration is directly related to the valency of the connectors. 19 For example, the 3-fold connected DG is less frustrated than the 4-fold connected DD, because more struts are connected to a single node in the DD, which makes its node bulkier. While packing frustration has received considerable attention as the origin of NET phase formation in diblock polymers, the extent to which the average mean curvature of the NET microstructure matches the spontaneous curvature of the interface produced by the block polymer also plays an important role in the morphology selection. 19,21 Moreover, the interfacial area per chain, which governs the amount of A/B contact, also contributes to phase selection. These three driving factors (packing frustration, curvature matching and area per chain) are not mutually exclusive, and thus makes a priori understanding of the basis for NET phase selection challenging.

In comparison with the well-studied cubic double NETs in block copolymer systems, there are no systematic reports on the stabilities of cubic single NETs, and detailed insight into their absence in block copolymers remain unclear. Herein, our objective is to examine the factors contributing to the stability of cubic single NETs in linear AB diblock copolymer melts using SCFT.

#### **METHODS**

#### SELF-CONSISTENT FIELD THEORY

SCFT is the most successful tool for investigating the phase behavior of block polymers, in particular for its ability to determine order-order transitions between different phases that are qualitatively in accord with experimental observations and its ability to do so in a computationally efficient manner. <sup>22</sup> In the present context, SCFT is an ideal tool to study single NETs for the following four reasons. First, the free energies of metastable phases can be readily calculated from converged SCFT solutions because different solutions of the self-consistent field equations are possible depending on the initial input for the fields. In most scenarios, as long as a reasonably good initial field is provided as the input, a converged solution for a structure of interest can be obtained. Second, SCFT provides easy access to the key parameters that affect mesophase morphology selection in block copolymers, allowing a systematic study of the effects of segregation strength and diblock copolymer composition on the relative stability of cubic single NETs. Third, the free energy calculated by SCFT can be decomposed into the enthalpic penalty from dissimilar polymer contacts and the entropy loss caused by chain stretching, allowing their relative effects to be readily compared. <sup>23</sup> Fourth, geometric analysis is relatively straightforward starting with an SCFT solution, because the interface at an equal volume fraction of the two blocks can be identified from the composition field of the SCFT solution. Mean curvature and other geometry-related calculations can then be conducted based on this surface. 19,21 These advantages are tempered, of course, by the mean-field approximation embedded in SCFT. For our purposes, the fluctuation effects neglected by SCFT are expected to be of minimal importance since we are comparing ordered phases, but one should be cautious if applying the results obtained here to systems with high self-concentration.<sup>24</sup>

Here, we provide a brief introduction to the underlying physics and governing equations of SCFT; the details about the theory and its implementation can be found in Refs. 18, 22, and 25. Our implementation of SCFT idealizes a polymer chain as a continuous Gaussian chain containing N coarse-grained monomers. Each monomer is indexed by a continuous contour variable s ranging from 0 to N, where s=0 and s=N represent the two ends of

the polymer chain. The chemical potential field that interacts with any monomer from the A block at position  $\mathbf{r}$ ,  $\omega_{A}(\mathbf{r})$ , is given by

$$\omega_{\mathcal{A}}(\mathbf{r}) = \chi \phi_{\mathcal{B}}(\mathbf{r}) + \xi(\mathbf{r}) \tag{1}$$

where  $\chi$  is the effective segmental interaction parameter,  $\phi_{\rm B}(\mathbf{r})$  stands for the local volume fraction of type B monomer at position  $\mathbf{r}$ , and  $\xi(\mathbf{r})$  is a Lagrange multiplier chosen to ensure that the volume fractions of all monomers sum to 1 at each position. For a diblock copolymer with volume fraction  $f_{\rm A}$ , the field  $\omega_{\rm A}(\mathbf{r})$  acts on segments from s=0 to  $s=f_{\rm A}N$ . A second chemical potential field,  $\omega_{\rm B}(\mathbf{r})$ , acts on segments from  $s=f_{\rm A}N$  to N. This second field is defined in a manner analogous to Eqn. 1 with the A and B subscripts interchanged.

With this construction,  $q(\mathbf{r}, \mathbf{s})$  is defined as a constrained partition function for a chain segment that starts at monomer 0 and ends at monomer s when monomer s is confined at position  $\mathbf{r}$ . The quantity  $q(\mathbf{r}, \mathbf{s})$  is also termed the "forward propagator". Similarly, a "backward propagator"  $q^{\dagger}(\mathbf{r}, \mathbf{s})$  can be defined where the chain segment begins at monomer N. The random-walk statistics of a polymer can then be described by the modified diffusion equations (MDEs) for the two propagators

$$\frac{\partial q(\mathbf{r}, s)}{\partial s} = \left[\frac{b^2}{6} \nabla^2 - \omega_i(\mathbf{r})\right] q(\mathbf{r}, s) \tag{2}$$

$$-\frac{\partial q^{\dagger}(\mathbf{r}, s)}{\partial s} = \left[\frac{b^2}{6} \nabla^2 - \omega_i(\mathbf{r})\right] q^{\dagger}(\mathbf{r}, s)$$
(3)

with initial conditions  $q(\mathbf{r}, 0) = q^{\dagger}(\mathbf{r}, N) = 1$ . Here, b is the statistical segment length, and i denotes the chemical identity for the segment of chain contour coordinate s. From the solutions for these propagators, the volume fraction at each position is calculated from

$$\phi_{\mathcal{A}}(\mathbf{r}) = \frac{1}{NQ} \int_0^{f_{\mathcal{A}}N} ds \ q(\mathbf{r}, s) q^{\dagger}(\mathbf{r}, s) \tag{4}$$

where

$$Q = \frac{1}{V} \int d\mathbf{r} \ q(\mathbf{r}, N) \tag{5}$$

is the partition function for an unconstrained chain and V is the unit-cell volume. From mass conservation, it follows that  $\phi_{\rm B}({\bf r}) = 1 - \phi_{\rm A}({\bf r})$ .

According to Eqn. 1, the chemical potential fields  $\omega_i(\mathbf{r})$  depend on the volume fractions  $\phi_i(\mathbf{r})$ . On the other hand, the volume fractions  $\phi_i(\mathbf{r})$  depend on the propagator functions

 $q(\mathbf{r}, s)$  and  $q^{\dagger}(\mathbf{r}, s)$  (Eqn. 4), which further depend on  $\omega_i(\mathbf{r})$  according to Eqns. 2-3. As a result, these equations need to be solved iteratively until self-consistency is achieved. In order to initialize the iteration scheme, an initial chemical potential or volume fraction field is required as an input, which is evolved using a quasi-Newton-Raphson iteration algorithm.<sup>22</sup>

Once a converged solution for a specific phase is obtained, the free energy per chain is calculated from

$$\frac{F}{nk_{\rm B}T} = -\ln(eQ) + \frac{\chi N}{V} \int d\mathbf{r} \, \phi_{\rm A}(\mathbf{r}) \phi_{\rm B}(\mathbf{r}) - \frac{N}{V} \int d\mathbf{r} \, \left[\omega_{\rm A}(\mathbf{r}) \phi_{\rm A}(\mathbf{r}) + \omega_{\rm B}(\mathbf{r}) \phi_{\rm B}(\mathbf{r})\right]$$
(6)

where  $k_{\rm B}T$  is the thermal energy and n is the total number of chains. The Helmholtz free energy per chain can be further decomposed as  $^{23}$ 

$$\frac{F}{nk_{\rm B}T} = \frac{U}{nk_{\rm B}T} - \frac{(S_J + S_{\rm A} + S_{\rm B})}{nk_{\rm B}}$$
 (7)

where U is the internal energy,  $S_J$  is the translational entropy of the AB junctions,  $S_A$  is the configurational entropy of the A block, and  $S_B$  is the entropy of the B block. The internal energy per chain is simply the second term in Eqn. 6,

$$\frac{U}{nk_{\rm B}T} = \frac{\chi N}{V} \int d\mathbf{r} \, \phi_{\rm A}(\mathbf{r}) \phi_{\rm B}(\mathbf{r}) \tag{8}$$

Since our model is incompressible, the internal energy is equal to the enthalpy. The configurational entropy per chain of the A block and B block can be calculated from <sup>23</sup>

$$-\frac{S_{A}}{nk_{B}} = -\frac{N}{V} \int d\mathbf{r} \left[ \rho_{J}(\mathbf{r}) \ln q(\mathbf{r}, s) + \omega_{A}(\mathbf{r}) \phi_{A}(\mathbf{r}) \right]$$
(9)

$$-\frac{S_{\rm B}}{nk_{\rm B}} = -\frac{N}{V} \int d\mathbf{r} \left[ \rho_J(\mathbf{r}) \ln q^{\dagger}(\mathbf{r}, s) + \omega_{\rm B}(\mathbf{r}) \phi_{\rm B}(\mathbf{r}) \right]$$
(10)

where  $\rho_J(\mathbf{r})$  is the distribution of the diblock junctions. These quantities can be understood as the chain-stretching penalties for each block. We do not report the chain junction entropy here, but it can be readily obtained from Eqn. 7.

Our SCFT calculations here were performed based on the open-source Polymer Self-Consistent Field software (PSCF) developed by Morse and coworkers. <sup>22</sup> PSCF uses a pseudo-spectral method to solve the MDEs. <sup>26</sup> In the pseudo-spectral method, periodic solutions of MDEs are discretized by a certain number of grid points in real space and a computational step  $\Delta s$  for the time-like contour length variable. The particular pseudospectral method

used in PSCF was developed by Ranjan et~al., <sup>27</sup> which provides fourth-order accuracy. An integration step size  $\Delta s = 0.01N$  was chosen for the input files in our calculations. For cases where the contour length step does not align with the block size, e.g.,  $f_{\rm A} = 0.305$ , PSCF selects a value of  $\Delta s$  that is as close as possible to that requested in the input file. A tolerance of  $10^{-5}$  for the convergence were used for all the calculations. The grid sizes used for all the cubic NETs were at least  $64 \times 64 \times 64$ , with higher resolutions of  $128 \times 128 \times 128$  and  $192 \times 192 \times 192$  used to resolve the interface for the geometric analysis.

#### FIELD INITIALIZATION

Converging the non-linear, non-local SCFT equations to a structure of interest requires that the fields be initialized with values that are within the basin of attraction for that morphology. In most cases, the chemical potential field of a previously converged SCFT solution of the desired structure can be used, which works well when the block polymer parameters are similar to a previous calculation.  $^{22}$  However, such converged PSCF solutions were not available for some of the cubic NETs. In these cases, we used a level-set method for generating initial fields for NETs.  $^{22,28}$  The simplest level-set method uses the first non-zero symmetry-adapted basis function of the specified space group and the desired volume fraction  $f_A$  to identify the dividing interface between A and B domain, and has been successfully applied to the DG phase.  $^{22}$  Unfortunately, this method fails for the DD and DP phases, as one basis function is not sufficient to capture the key features of their complex morphologies. Inspired by the work by Wohlgemuth  $et~al.^{29}$ , we used multiple basis functions to reconstruct the geometric models for these phases, which successfully converged to the desired structures. The prefactors for the combinations of basis functions can be found in Ref. 29.

#### **GEOMETRIC ANALYSIS**

We performed the mean curvature calculations from our converged SCFT solutions using a modified version of the software originally developed by Feng et al.<sup>30</sup> In our sightly modified version of their program, the domain interface is identified as the surface where  $\phi_{\rm A}(\mathbf{r}) = \phi_{\rm B}(\mathbf{r}) = 0.5$ . The surface is represented by a triangulated mesh, which is identified by a linear interpolation of the composition field generated from converged SCFT solutions. Instead of

performing the two-step conditioning in their software package, we instead increased the resolutions of the triangulated mesh to reduce the error caused by irregular edge lengths and roughness of the mesh. As shown in Figure S1, a mesh with over  $10^5$  vertices can be used to compute curvatures and interfacial areas with small absolute errors ( $10^{-3}$  and  $10^{-4}$ , respectively). The mean curvature  $H = (k_1 + k_2)/2$  on each triangulated vertex can be obtained once the principle curvatures  $k_1$  and  $k_2$  are calculated. A positive principle curvature indicates the interface is curved towards the B domain. The total interfacial area A is calculated by summing the area of all the triangles in the mesh, which is then normalized by the volume of the unit cell.

#### **RESULTS AND DISCUSSION**

The phase behavior of conformationally symmetric linear AB diblock copolymer melts ( $b_A = b_B$ ) in the mean-field limit is determined by two factors: the degree of segregation  $\chi N$  between A and B segments and the volume fraction of the A block,  $f_A$ .<sup>18,19</sup> Increasing  $f_A$  towards the symmetric composition leads to a phase transition  $C \to DG \to L$  in most regions of the morphology diagram. The key exception that is relevant for our work is an orthorhombic single NET with Fddd symmetry,  $O^{70}$ , that was predicted to be stable near the DG/L phase boundary at low  $\chi N$ , and later confirmed by experiments.<sup>31,32</sup> In what follows, we will work at values of  $\chi N$  such that  $O^{70}$  is always higher in free energy than DG.

Although it is believed that cubic single NETs are metastable in block copolymers, the free energies of cubic single NETs have not been systematically reported even for the simplest linear diblock copolymer melts. Thus, we begin by computing the free energies of cubic single NETs in a 2-D parameter space of  $\chi N$  and  $f_A$  using SCFT. An upper limit of  $\chi N=40$  was chosen for computational efficiency; increasing  $\chi N$  increases the computational costs since more grid points are required to accurately resolve the sharpened interface. The lower limit for our calculations is either the order-disorder transition or the DG- $O^{70}$  order-order transition, such that DG is the stable network phase. The range of  $f_A$  spans from 0.3 to 0.5, which covers the entire NET-forming region, as well as some regions of C and L. Our results confirm, as expected, that all three cubic single NETs are metastable phases throughout the

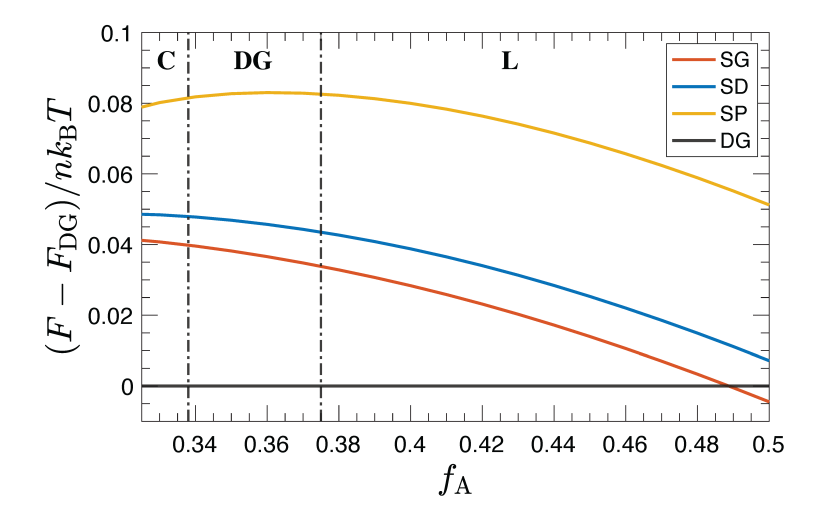


Figure 2: Helmholtz free energy per chain of cubic single NETs relative to the free energy of the DG phase in diblock copolymer melts at  $\chi N = 20$  as a function of composition  $f_A$ . The dash-dot lines indicate the C/DG and DG/L phase boundaries, respectively. The notation at the top of the panel indicates the stable phase.

whole parameter space that we studied. By way of example, Figure 2 shows the free energy differences between cubic single NETs and DG at  $\chi N=20$ . The equivalent figures  $\chi N=30$  and  $\chi N=40$  are provided in Fig. S2. In the DG-forming region, the cubic single NETs are at least  $0.034~nk_{\rm B}T$  higher than DG in free energy, indicating that the cubic single NETs are of sufficiently higher free energy that they are likely inaccessible by non-equilibrium processing methods and unlikely to be stabilized by fluctuations. One interesting observation is that the free energy of SG crosses below the free energy of DG near the symmetric composition where L is the equilibrium phase; we will return to this point later. However, the excess free energies of SG and SD, i.e., the energy differences between the metastable phase and the stable phase, are minimized at  $f_{\rm A}=0.375$ , because L becomes the equilibrium state at more symmetric compositions, suggesting that any modifications to the molecular design intended to produce SG or SD are most likely to succeed near the DG/L boundary.

#### RELATIVE STABILITIES OF CUBIC SINGLE NETS

Confirming that none of the cubic single NETs is a stable phase in diblock copolymer melts, our focus now moves to investigating the relative stability of the cubic NET phases to

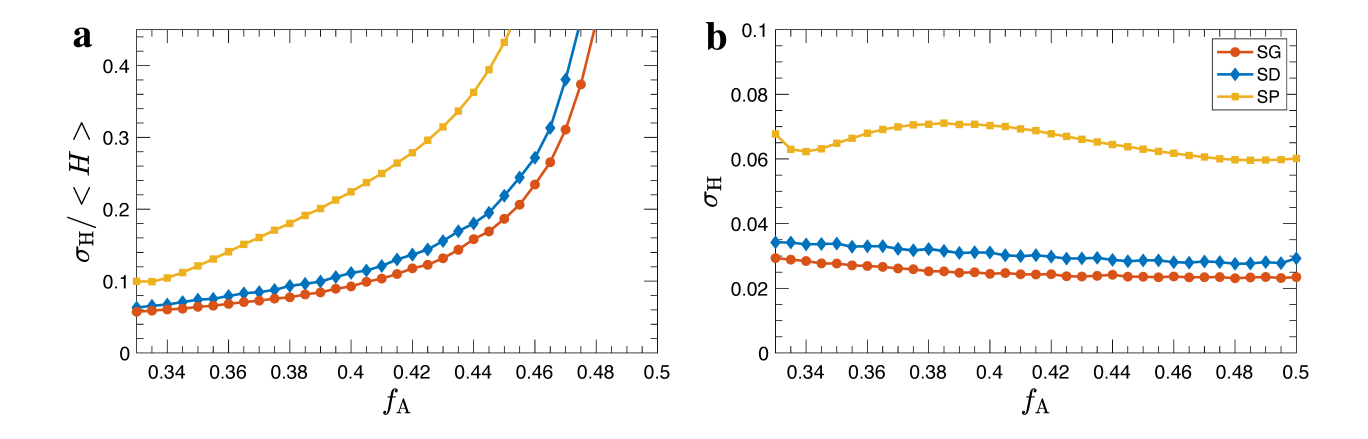


Figure 3: (a) Relative variation and (b) standard deviation in mean curvature of the domain interface of the cubic single NETs as a function of diblock copolymer composition  $f_{\rm A}$  at  $\chi N=20$ . The unit for  $\sigma_{\rm H}$  is  $1/\sqrt{N}b$ .

understand the origin of that metastability. As we discussed earlier, the packing frustration argument has successfully explained the origins of double NET morphology selection in block copolymers. <sup>19,23</sup> Hence,  $\sigma_{\rm H}/\langle H \rangle$  has been used to measure the inability of the double NETs to simultaneously minimize interfacial area and chain stretching.

The results of our free energy calculation of cubic single NETs are consistent with the argument for the double networks, i.e., that higher valency connectors increase packing frustration. As shown in Figure 2, the 3-fold connected SG has the lowest free energy, while the 6-fold connected SP has the highest free energy among the three single NETs. Figure 3(a) provides the relative variation in mean curvature  $\sigma_{\rm H}/\langle H\rangle$  of the cubic single NETs, showing a trend consistent with the free energy calculations. Note that the  $\sigma_{\rm H}/\langle H\rangle$  curves of the cubic single NETs diverge when approaching the symmetric composition because the domain interface is approaching the triply periodic minimal surface geometry. The mean curvature of a minimal surface is zero everywhere, which means its average mean curvature  $\langle H\rangle=0.^{33}$  Thus, it is more straightforward to directly compare the standard deviation of mean curvature  $\sigma_{\rm H}$  here, given that the  $\langle H\rangle$  of the single NETs are not substantially different from one another, as shown in Figure S3. Figure 3(b) illustrates  $\sigma_{\rm H}$  for the three structures, producing the same free energy order SG  $\langle SD \rangle \langle SP \rangle$ . Moreover, the differences in  $\sigma_{\rm H}$  between SG and SD are smaller compared to the differences between SD and SP. This trend

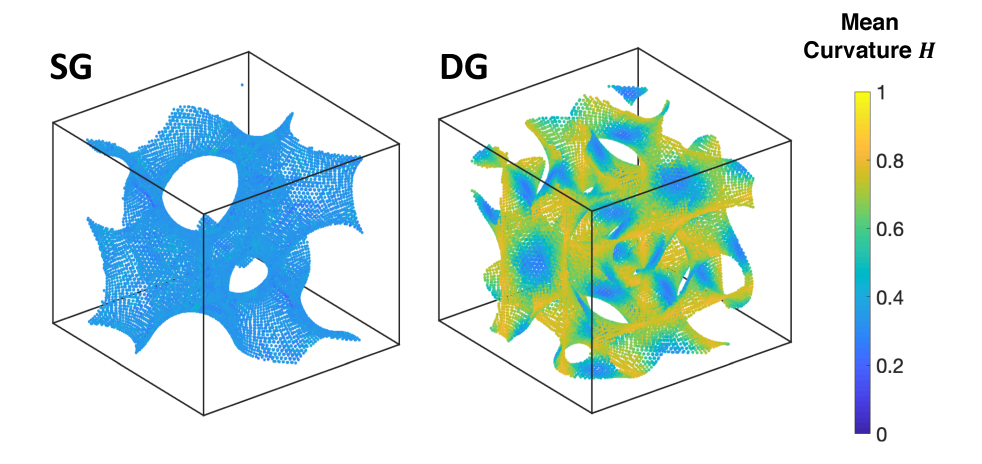


Figure 4: Mean curvature maps of SG and DG in diblock copolymer melts at  $f_A = 0.4$  and  $\chi N = 20$ . The color on the vertex of the triangulated mesh indicates the mean curvature at that point. The curvatures are scaled by  $1/\sqrt{N}b$ . The corresponding curvature distributions are provided in Figure S4 of Supplementary Information.

is also observed in the free energy differences in Figure 2, consistent with the idea that packing frustration is the dominant factor that affects the relative stability among cubic single NETs.

#### RELATIVE STABILITY BETWEEN CUBIC SINGLE AND DOUBLE NETS

Although the relative stability among the cubic single NETs is successfully explained by the packing frustration argument, the reason why the 3-fold connected DG is more stable than the 3-fold connected SG turns out to be inconsistent with the packing frustration principle. To see why, we apply the same mean curvature calculations to compare cubic single NETs with double NETs. The SG and DG structures are examined first since they have the lowest free energy among cubic single and double NETs, respectively, making SG the most promising single NET. The variation in mean curvature of DG is significantly larger than that of SG, as illustrated in Figure 4, even though SG has a higher free energy. Looking at the trends as a function of  $f_A$ , Figure 5(a) shows that  $\sigma_H/\langle H\rangle$  of SG is smaller than that of the DG except for the high  $f_A$  region where the  $\langle H\rangle$  of SG is close to zero. Again, we compare the  $\sigma_H$  directly in Figure 5(b) to avoid the divergence of the single NETs at symmetric composition, and observe that the standard deviation in mean curvature of DG

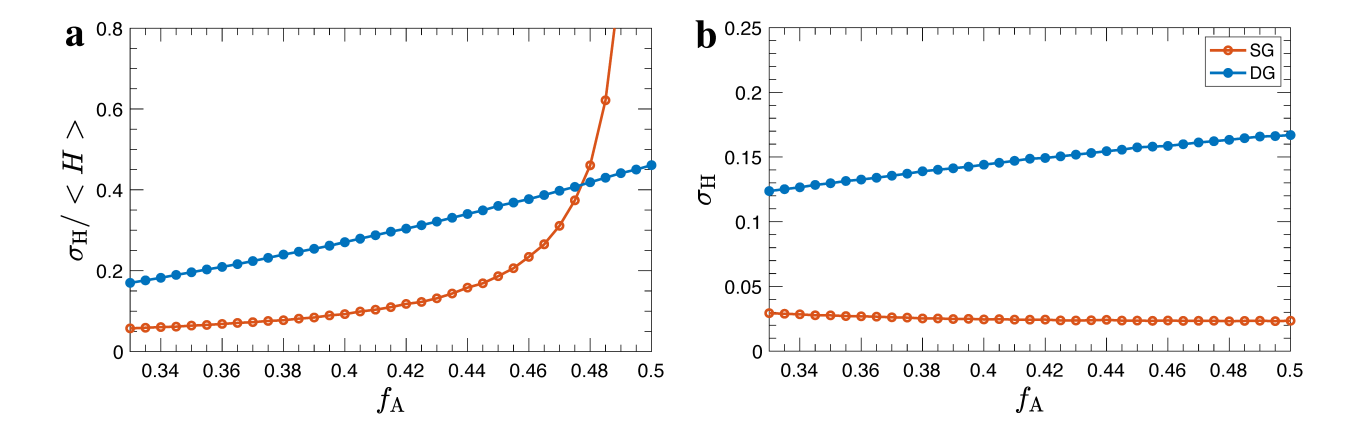


Figure 5: Comparison of packing frustration for DG and SG at  $\chi N = 20$ . (a) Relative variation and (b) standard deviation in mean curvature of the domain interface of the SG and DG phases as a function of diblock copolymer composition  $f_A$ . The unit for  $\sigma_H$  is  $1/\sqrt{N}b$ .

is at least three times greater than that of SG. These results contradict the previous packing frustration argument based on curvature variation, meaning that other factors beyond this standard definition for packing frustration <sup>19</sup> suppress the formation of SG relative to DG.

In order to explore the possible factors that dominate the morphology selection of DG over SG, we first examine how well  $\langle H \rangle$  of the domain interface of the microstructures matches their preferred curvatures. There are various models that describe the structural features of a specific microstructure, and the simplest such model is the level set model that uses the first non-zero symmetry-adapted basis function. The preferred curvature of a microstructure at a specific volume fraction can be estimated by the  $\langle H \rangle$  of the interface from the level set model. Thus, we compared the  $\langle H \rangle$  from the level set models and SCFT solutions of both SG and DG. As shown in Figure 6(a) in the DG-forming region, the interfacial curvature differences from the two models is smaller for DG, indicating that the DG is favored in terms of curvature matching at this value of  $\chi N$ .

The interfacial tension may be another factor that leads to the selection of DG over SG. In strong segregation theory, the interfacial tension is directly related to the interfacial area and thus the enthalpy resulting from dissimilar polymer segment contacts.<sup>34</sup> In the intermediate-segregation regime under study here, the interfacial width (and the way in which the local

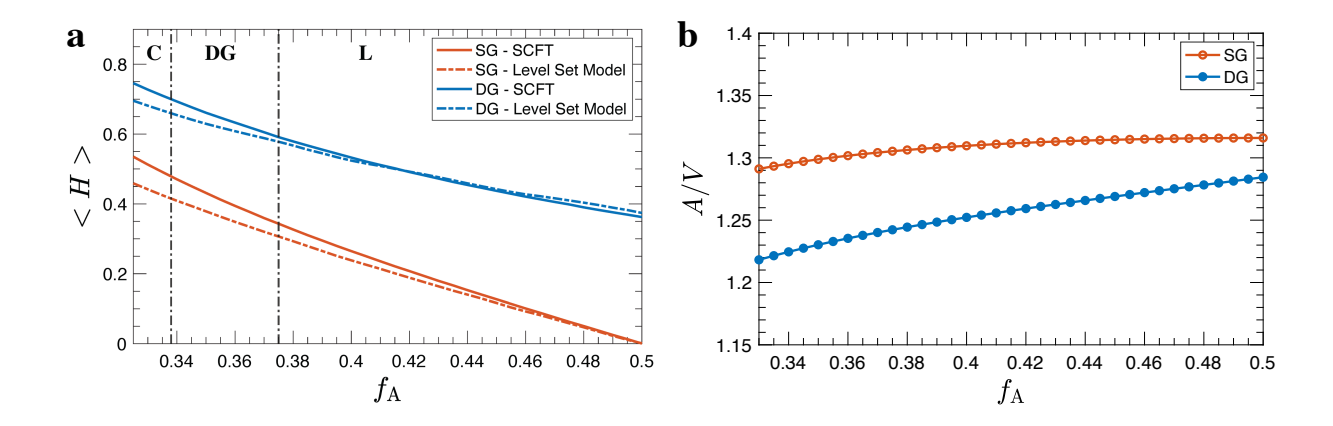


Figure 6: (a) Average mean curvature from SCFT solutions and level set models and (b) interfacial area per unit volume of the SG and DG phases as a function of composition  $f_A$ . Both the  $\langle H \rangle$  and A/V are scaled by  $1/\sqrt{N}b$ .

volume fractions  $\phi_A(\mathbf{r})$  and  $\phi_B(\mathbf{r})$  vary across that width) must also be considered because the interface is diffuse. <sup>23</sup> Since the interfacial width (e.g., the distance between regions where  $\phi_A = 0.9$  and  $\phi_A = 0.1$ ) of two different structures for the same segregation strength should not differ by much, we decided to examine the interfacial area per unit volume of SG and DG to see if it causes the difference in enthalpy. The results are shown in Figure 6(b), where we see that the interfacial area per unit volume of SG is indeed higher than that of DG at all compositions, indicative of a higher interfacial tension of SG.

To more completely understand the thermodynamic origins of the stability of DG over SG, we further decompose the Helmholtz free energy to the enthalpic contribution  $U/nk_{\rm B}T$  and the entropic contribution  $-S/nk_{\rm B}$ . As shown in Figure 7, even though the domain interface of SG is more CMC-like (because  $\sigma_{\rm H}/\langle H\rangle$  of SG is smaller, except for the nearly symmetric compositions where L is the stable state), SG still has a higher enthalpy compared to DG, which supports the argument that the effective interfacial tension of SG is higher because of the higher interfacial area per unit volume. In contrast, the entropic contribution for DG is higher, which is mainly caused by the higher degree of packing frustration of DG. We note that the deviation from the preferred curvature in Figure 6(a) reflects both enthalpic and entropic contributions that cannot be cleanly nor easily deconvoluted when compared to the ease in analyzing A/V. Figure 7 also shows that the competition between DG and

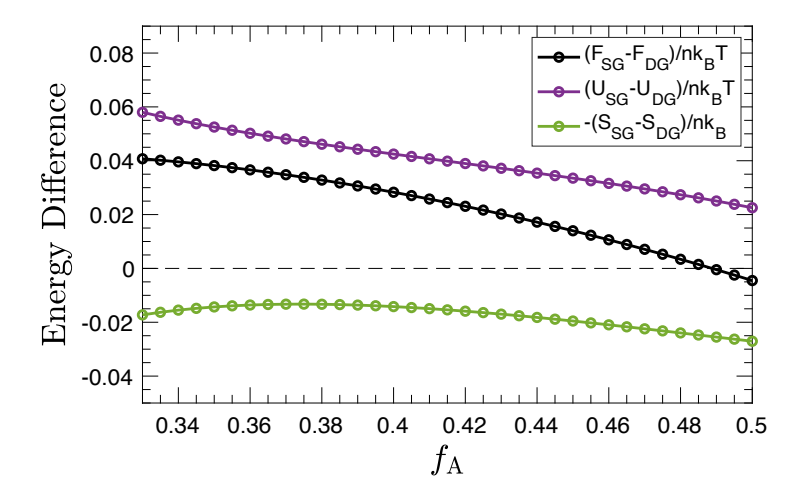


Figure 7: Differences between the SG and DG phases in Helmholtz free energy per chain, enthalpic contribution, and entropic contribution to the free energy as a function of diblock copolymer composition  $f_A$  at  $\chi N = 20$ .

SG is more strongly impacted by the enthalpy, and this competition results in a positive free energy difference  $F_{SG} - F_{DG}$ .

These results indicate that an area-minimized surface (CMC surface) does not guarantee a lower enthalpy nor a better curvature matching, and thus we propose a different mechanism of relieving packing frustration for the cubic single NETs. While the cubic double NETs deviate from the CMC surface to compensate for the chain stretching, the cubic single NETs instead tend to shrink their domain sizes and maintain the CMC structure, which is evidenced by the cubic lattice parameters provided in Figure S5. A decrease in domain size leads to an increase in the interfacial area per unit volume of cubic single NETs, which causes an increase in enthalpic penalties.

The effect of increasing  $f_A$  also differs for the single and double networks. Figure 6(b) shows that interfacial area per unit volume of DG increases as  $f_A$  increases, owing to the further deviation from the CMC surface of DG caused by the increased chain-stretching penalties, where this deviation is evidenced by the increase in  $\sigma_H$  of DG with increasing  $f_A$  in Figure 5(b). The entropic penalties increase because the DG node increases in volume when  $f_A$  increases, making the double NET sensitive to the polymer composition. This behavior is similar to that observed in lyotropic liquid crystals, where the relative stability of DG versus

DD and DP decreases as the volume fraction of the cable networks increases.<sup>35</sup> For SG, however, changing the composition shifts the interface to enclose a different network volume, but does not change the CMC-like geometry of the surface. Also, because SG contains one network in each domain, increasing the size of the network node in the A domain decreases the size of the node in the B domain, which makes SG less sensitive to change of composition. Moreover, curvature matching is less of a problem for SG near  $f_A = 0.5$  as indicated by the smaller curvature differences in Figure 6(a). This can explain why the free energy of SG becomes lower than that of DG near  $f_A = 0.5$  as shown in Figure 7. Although the L phase is the equilibrium phase in that region, the fact that SG is favorable over DG makes us wonder if certain polymer architecture that destabilizes the L phase can lead to a formation of SG. Indeed, a recent paper by Xie et al. <sup>10</sup> has predicted a stabilization of SG in a more complicated BABAB pentablock copolymer system, which indicates the feasibility of this idea.

To ensure our discussion of the SG metastability based on interfacial area is valid not only at a relatively low  $\chi N$ , we performed similar analyses at  $f_{\rm A}=0.38$  with a varied  $\chi N$  ranging from 15 to 60 in Figure 8. Over this range of  $\chi N$ , the curvature matching fails to explain the stabilization of DG since the curvature difference of DG is larger for most  $\chi N$  as shown in Figure 8(b), even though this was a case where the preferred curvature of DG was very closely matched by the SCFT solution at  $\chi N=20$  in Figure 6(a). Hence, the curvature matching concept cannot fully explain the metastability of SG. Rather, the enthalpic contribution caused by the larger interfacial area per unit volume (Fig. 8(b)) remains the main cause of the metastability of SG over the full range of  $\chi N$ . The decrease in  $\sigma_{\rm H}/\langle H\rangle$  (Fig. 8(a)) and the increase in interfacial area per unit volume for both structures caused by the increasing segregation strength are consistent with the earlier study by Matsen. <sup>23</sup> Moreover, the gap between  $\Delta U/nk_{\rm B}T$  and  $-\Delta S/nk_{\rm B}$  becomes smaller as  $\chi N$  increases, as shown in Figure 8(d), indicating that the chain stretching entropy is playing a more important role at higher segregation strengths. This observation, together with the finding that a more CMC-like shape is preferred at weak segregation, agrees with previous observations by Feng et al. <sup>21,30</sup>

We also performed similar calculations for the SD and DD phases to evaluate the packing frustration and effective interfacial tension, shown in Figure S6, and the conclusions we drew

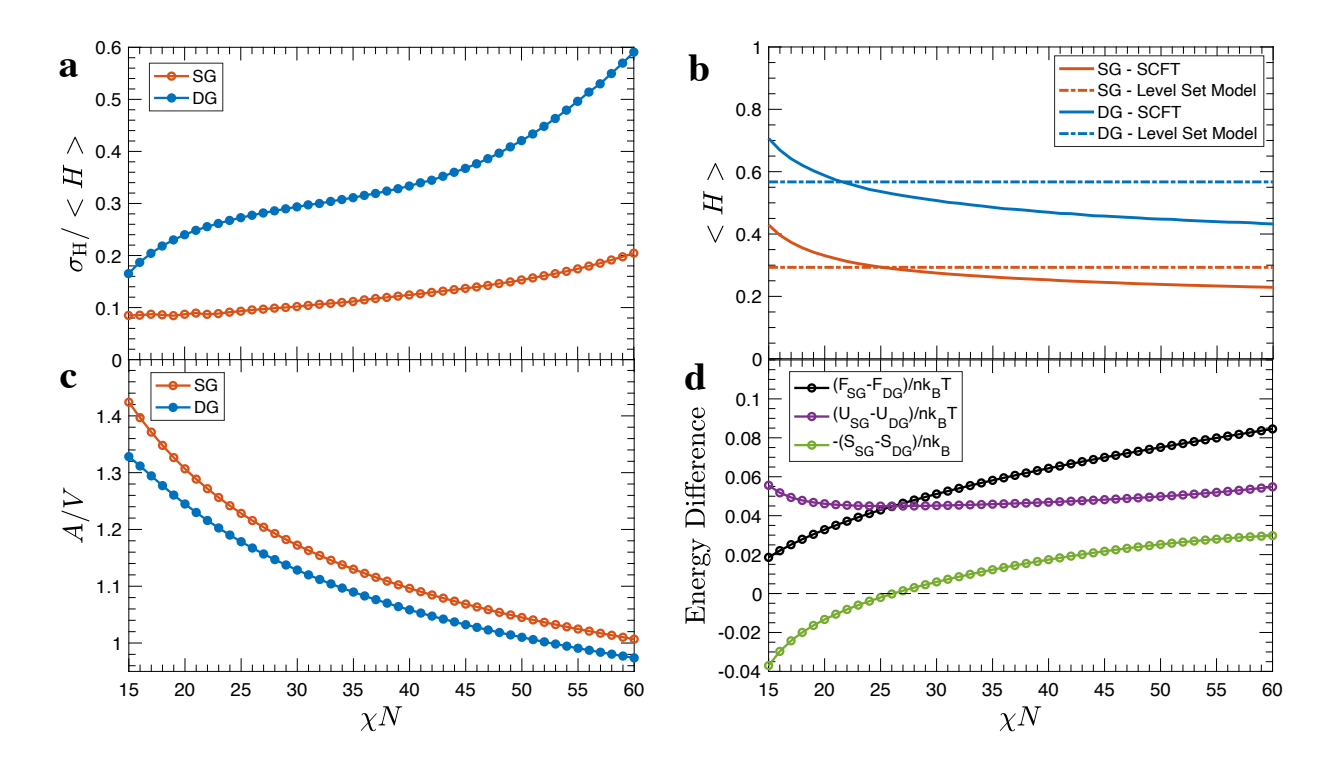


Figure 8: Comparison of DG and SG as a function of  $\chi N$  for  $f_{\rm A}=0.38$ . (a) Relative variation in curvature, (b) average mean curvature from SCFT solutions and level set models, and (c) interfacial area per unit volume of the SG and DG phases. Both the  $\langle H \rangle$  and A/V are scaled by  $1/\sqrt{N}b$ . (d) Differences between the SG and DG phases in Helmholtz free energy per chain, enthalpic contribution, and entropic contribution to the free energy.

from the comparisons between DG and SG translate to this other network. The SP is of less interest, since the free energy of SP is much higher compared to the other cubic single NETs, so we did not extend our analysis further due to the computational cost of the geometric analysis. We thus conclude that the major cause of the metastability of the cubic single NETs is the higher enthalpic penalty originating from the larger interfacial area per unit volume, rather than packing frustration or matching of the preferred interfacial curvature.

#### CONCLUSIONS

In the present contribution, we implemented a series of free energy comparisons and geometric analyses based on SCFT calculations to study the stabilities of cubic single NETs in linear diblock copolymer melts. Analyses of the resulting free energies confirm the metastability of the cubic single NETs, and also show that SG and SD phases are least metastable at the DG/L boundary. Moreover, while the packing frustration argument based on measuring the variation in mean curvature successfully describes the free energy relations between the cubic single NETs, it fails when applied to the comparisons between cubic single and double NETs. The curvature matching between the averaged mean curvature of the microstructure and spontaneous curvature of the domain interface also is not a major factor that stabilizes cubic double NETs rather than single NETs, since this argument fails at strong segregation strength. Rather, the metastability of the cubic single NETs mainly arises from the larger enthalpic penalties originating from the large interfacial area per unit volume, even though the shapes of their domain interfaces are more CMC-like compared to that of the cubic double NETs. These results suggest that cubic single NETs tend to exhibit reduced domain sizes to compensate for chain-stretching penalties while maintaining nearly constant mean curvatures. While our measurements of deviations in interfacial curvature are the classical way to understand packing frustration, <sup>19</sup> measurements of skeletal thickness as well as medial thickness of the network domains may provide even deeper insights into the origins of the free energy differences between cubic single and double NETs. <sup>21</sup>

#### **ACKNOWLEDGMENTS**

This work was supported primarily by the National Science Foundation through the University of Minnesota MRSEC under Award Number DMR-2011401 and partially by Award Number DMR-1719692. The Minnesota Supercomputing Institute (MSI) at the University of Minnesota provided resources that contributed to the research results reported within this paper.

#### **CONFLICT OF INTEREST**

The authors declare no conflicts of interest.

### References

- 1. H. Kim and C. Leal, ACS Nano 9, 10214 (2015).
- E. J. Crossland, M. Kamperman, M. Nedelcu, C. Ducati, U. Wiesner, D. M. Smilgies,
   G. E. Toombes, M. A. Hillmyer, S. Ludwigs, U. Steiner, et al., Nano Lett. 9, 2807 (2009).
- 3. L. Yan, C. Rank, S. Mecking, and K. I. Winey, J. Am. Chem. Soc. 142, 857 (2020).
- G. L. Jackson, D. V. Perroni, and M. K. Mahanthappa, J. Phys. Chem. B 121, 9429 (2017).
- 5. B. A. Pindzola, J. Jin, and D. L. Gin, J. Am. Chem. Soc. **125**, 2940 (2003).
- L. Li, L. Schulte, L. D. Clausen, K. M. Hansen, G. E. Jonsson, and S. Ndoni, ACS Nano 5, 7754 (2011).
- 7. L. Han and S. Che, Adv. Mater. **30**, 1705708 (2018).
- 8. A. J. Meuler, M. A. Hillmyer, and F. S. Bates, Macromolecules 42, 7221 (2009).
- 9. T. Oka, N. Ohta, and S. T. Hyde, Langmuir **36**, 8687 (2020).
- 10. Q. Xie, Y. Qiang, and W. Li, ACS Macro Lett. 11, 205 (2022).
- 11. K. Michielsen and D. G. Stavenga, J. R. Soc. Interface 5, 85 (2008).
- 12. V. Saranathan, C. O. Osuji, S. G. Mochrie, H. Noh, S. Narayanan, A. Sandy, E. R. Dufresne, and R. O. Prum, Proc. Natl. Acad. Sci. U. S. A. 107, 11676 (2010).
- V. Saranathan, A. E. Seago, A. Sandy, S. Narayanan, S. G. J. Mochrie, E. R. Dufresne,
   H. Cao, C. O. Osuji, and R. O. Prum, Nano Lett. 15, 3735 (2015).
- 14. A. E. Seago, P. Brady, J. P. Vigneron, and T. D. Schultz, J. Roy. Soc. Interface 6, S165 (2009).
- 15. M. Maldovan, A. M. Urbas, N. Yufa, W. C. Carter, and E. L. Thomas, Phys. Rev. B Condens. Matter Mater. Phys. 65, 165123 (2002).

- S. Vignolini, N. A. Yufa, P. S. Cunha, S. Guldin, I. Rushkin, M. Stefik, K. Hur, U. Wiesner, J. J. Baumberg, and U. Steiner, Adv. Mater. 24, OP23 (2012).
- C. Kilchoer, N. Abdollahi, J. A. Dolan, D. Abdelrahman, M. Saba, U. Wiesner,
   U. Steiner, I. Gunkel, and B. D. Wilts, Adv. Opt. Mater. 8, 1902131 (2020).
- 18. M. W. Matsen and M. Schick, Phys. Rev. Lett. 72, 2660 (1994).
- 19. M. W. Matsen and F. S. Bates, Macromolecules **29**, 7641 (1996).
- 20. H. Hasegawa, T. Hashimoto, and S. T. Hyde, Polymer **37**, 3825 (1996).
- 21. A. Reddy, X. Feng, E. L. Thomas, and G. M. Grason, Macromolecules 54, 9223 (2021).
- 22. A. Arora, J. Qin, D. C. Morse, K. T. Delaney, G. H. Fredrickson, F. S. Bates, and K. D. Dorfman, Macromolecules 49, 4675 (2016).
- 23. M. W. Matsen and F. S. Bates, J. Chem. Phys. **106**, 2436 (1997).
- R. M. Lewis, A. Arora, H. K. Beech, B. Lee, A. P. Lindsay, T. P. Lodge, K. D. Dorfman, and F. S. Bates, Phys. Rev. Lett. 121, 208002 (2018).
- 25. M. W. Matsen, J. Phys. Condens. Matter 14, R21 (2002).
- 26. K. Ø. Rasmussen and G. Kalosakas, J. Polym. Sci. B: Polym. Phys. 40, 1777 (2002).
- 27. A. Ranjan, J. Qin, and D. C. Morse, Macromolecules **41**, 942 (2008).
- 28. E. W. Cochran, Thermodynamics, simulation, and modeling of ordered linear ABC triblock copolymers (PhD. Thesis, University of Minnesota, 2004).
- 29. M. Wohlgemuth, N. Yufa, J. Hoffman, and E. L. Thomas, Macromolecules **34**, 6083 (2001).
- 30. X. Feng, C. J. Burke, M. Zhuo, H. Guo, K. Yang, A. Reddy, I. Prasad, R. M. Ho, A. Avgeropoulos, G. M. Grason, et al., Nature 575, 175 (2019).
- 31. C. A. Tyler and D. C. Morse, Phys. Rev. Lett. 94, 208302 (2005).

- 32. M. Im Kim, T. Wakada, S. Akasaka, S. Nishitsuji, K. Saijo, H. Hasegawa, K. Ito, and M. Takenaka, Macromolecules **42**, 5266 (2009).
- 33. A. H. Schoen, *Infinite periodic minimal surfaces without self-intersections* (National Aeronautics and Space Administration, 1970).
- 34. A. Semenov, Macromolecules **26**, 6617 (1993).
- 35. H. Chen and C. Jin, Interface Focus 7, 20160114 (2017).

# Supplementary Information: Stability of Cubic Single Network Phases in Diblock Copolymer Melts

PENGYU CHEN, MAHESH K. MAHANTHAPPA, KEVIN D. DORFMAN\*

Department of Chemical Engineering and Materials Science, University of Minnesota – Twin Cities, 421 Washington Ave. SE, Minneapolis, MN 55455, USA.

\*Corresponding Author: Kevin D. Dorfman. Email: dorfman@umn.edu. Phone: +1-612-624-5560. Fax: +1-612-626-7246.

Dated: June 3, 2022

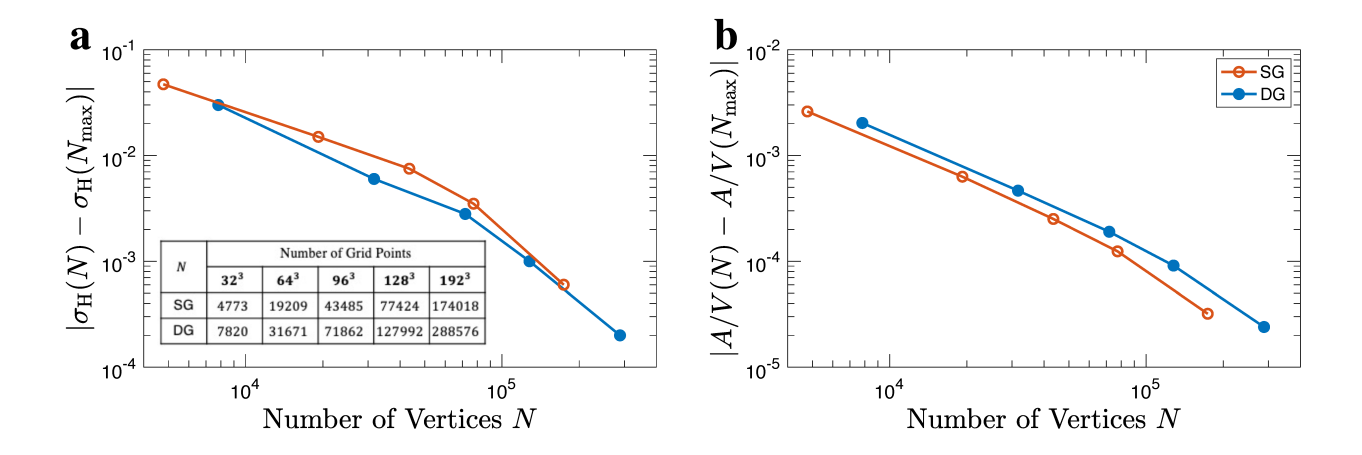


Figure S1: Absolute differences of (a) standard deviation in mean curvature (b) interfacial area per unit volume of the domain interface of the SG and DG phases with different number of vertices of the triangulated mesh. The highest resolution in the calculations,  $N_{\text{max}}$ , is used for comparison.  $N_{\text{max}}$  is about  $5 \times 10^5$  for DG and  $3 \times 10^5$  for SG. The values are different because the number of vertices of the triangulated mesh is not pre-specified, instead the number of grid points in the composition field is provided. The number of grid points is increased in order to increase the number of vertices in these calculations.

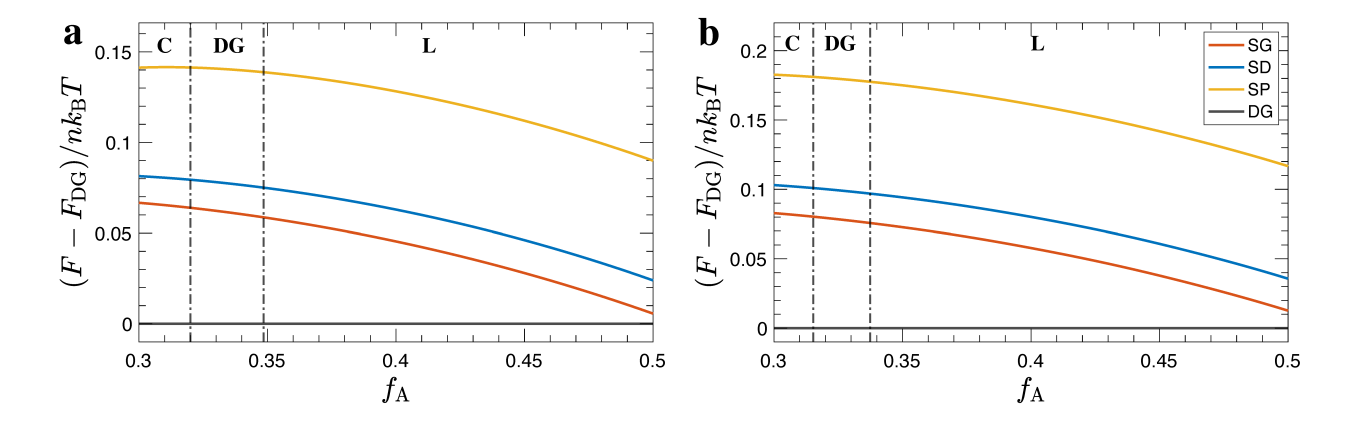


Figure S2: Helmholtz free energy per chain of cubic single NETs relative to the free energy of the DG phase in diblock copolymer melts at (a)  $\chi N = 30$  (b)  $\chi N = 40$  as a function of composition  $f_A$ . The dash-dot lines indicate the C/DG and DG/L phase boundaries, respectively. The notation at the top of the panel indicates the stable phase.

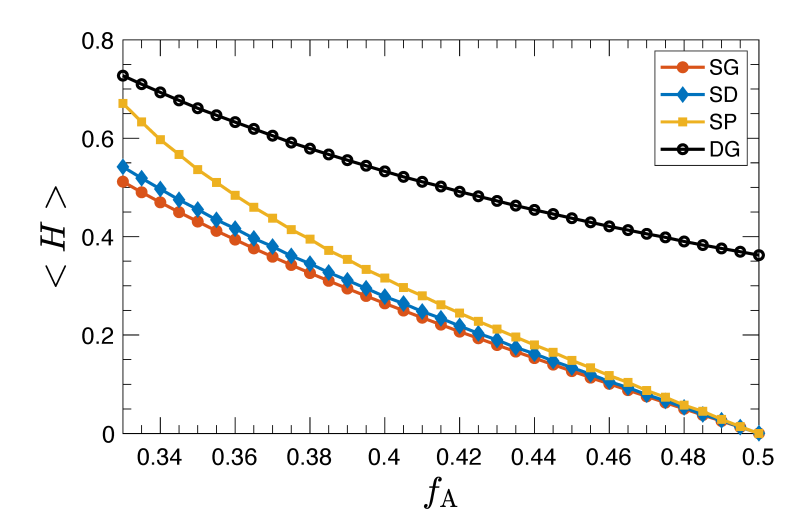


Figure S3: Average mean curvature of the domain interface of the cubic single NETs as a function of diblock copolymer composition  $f_A$  at  $\chi N = 20$ . Average mean curvature of DG is also shown for comparison.

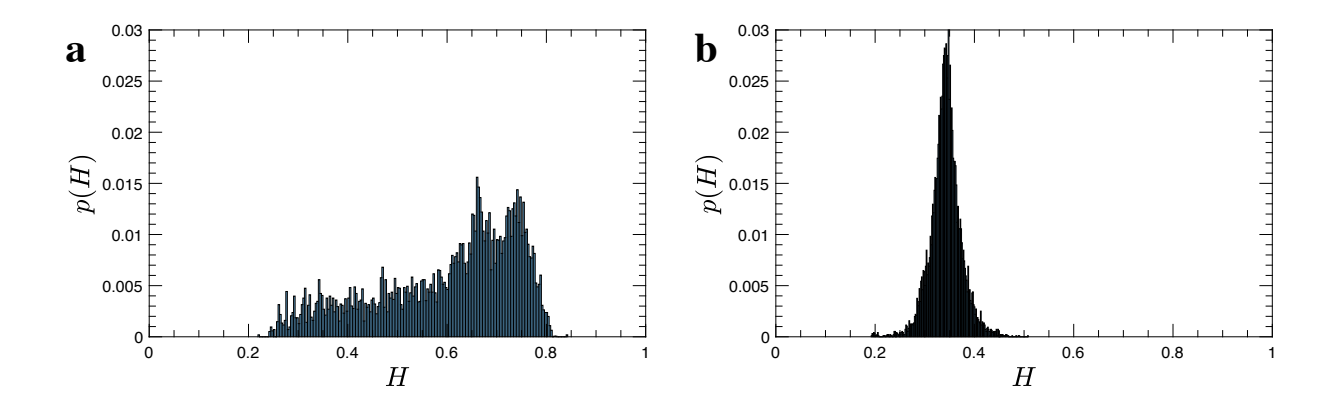


Figure S4: Local mean curvature distributions of (a) DG and (b) SG in diblock copolymer melts at  $f_{\rm A}=0.4$  and  $\chi N=20$ .

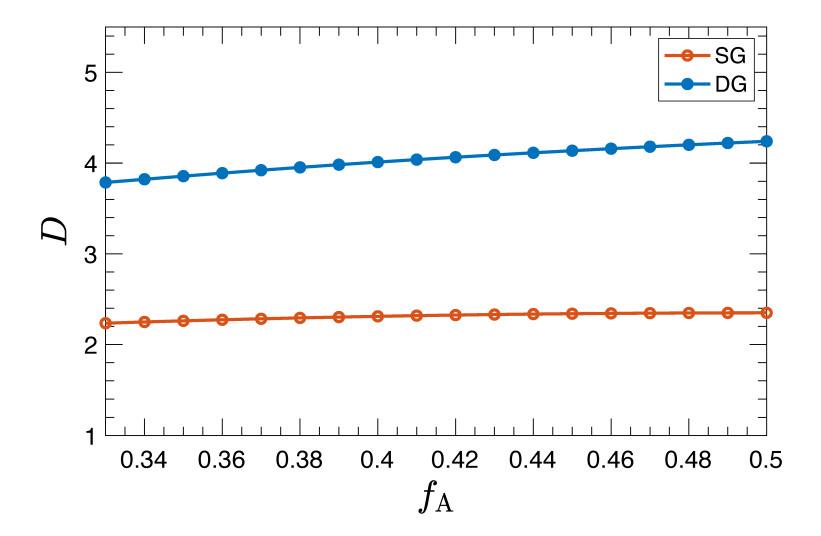


Figure S5: Cubic lattice parameters of SG and DG in diblock copolymer melts as a function of composition  $f_{\rm A}$  at  $\chi N=20$ .

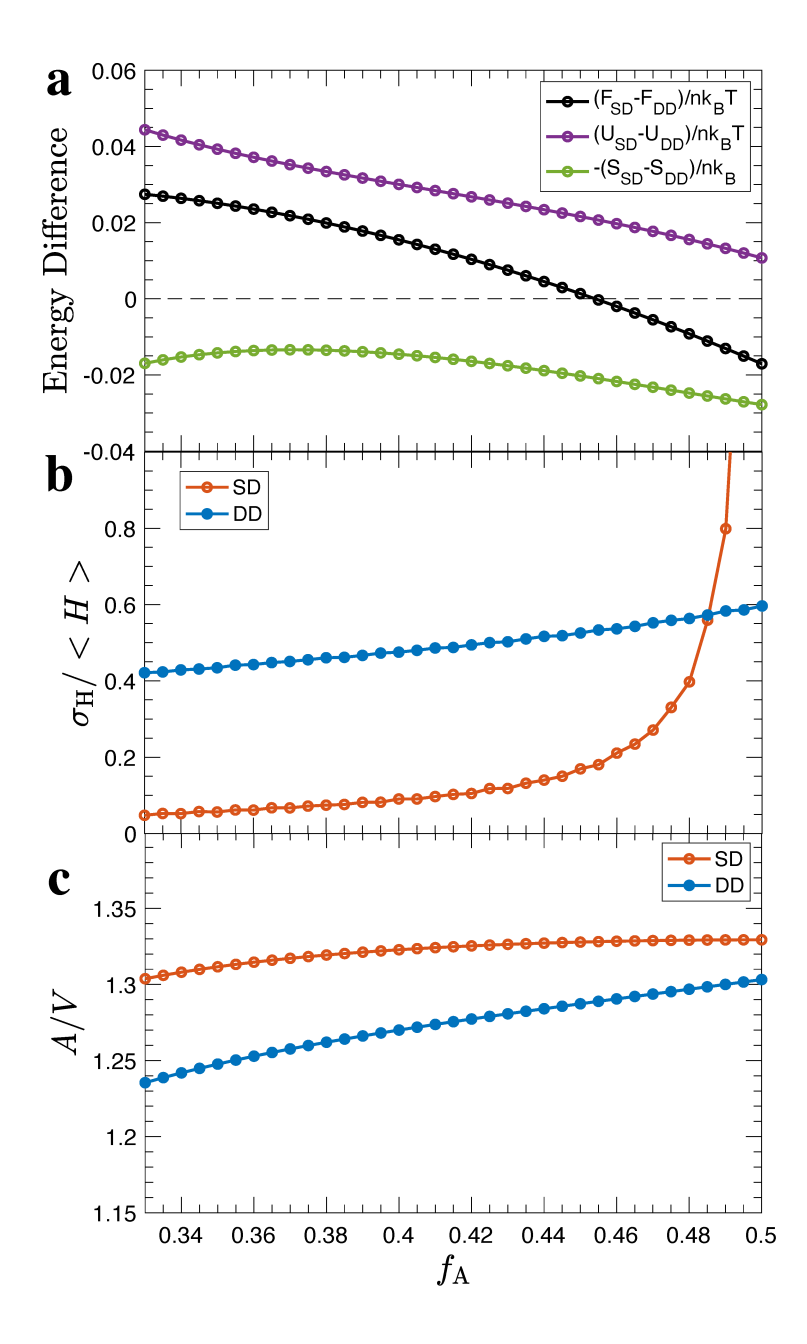


Figure S6: (a) Differences between the SD and DD phases in Helmholtz free energy per chain, enthalpic contribution, and entropic contribution to the free energy as a function of diblock copolymer composition  $f_{\rm A}$  at  $\chi N=20$ . (b) Relative variation in curvature and (c) interfacial area per unit volume of the SD and DD phases as a function of composition  $f_{\rm A}$  at  $\chi N=20$ .